Intermetallics 50 (2014) 43–53

Contents lists available at ScienceDirect

Intermetallics

journal homepage: www.elsevier.com/locate/intermet

Microstructure development during pack aluminization of nickel and nickel–chromium wires

Dinc Erdeniz*, David C. Dunand

Department of Materials Science and Engineering, Northwestern University, 2220 Campus Drive, Evanston, IL 60208, USA

ARTICLE INFO

Article history:
Received 12 December 2013
Received in revised form
10 February 2014
Accepted 14 February 2014
Available online 12 March 2014

Keywords:
A. Intermetallics
B. Age-hardening
B. Diffusion
C. Coatings
D. Microstructure

ABSTRACT

Pack aluminization – a chemical vapor deposition process widely used to form protective coatings on Ni-based superalloy components – was used to form shells of Ni_2Al_3, NiAl and/or γ′-Ni_3Al on the surface of γ-Ni wires with diameters of 127 μm. The growth kinetics of these Al-rich intermetallic shells are studied as a function of aluminization time and pack activity at 1000 °C. Similar kinetics but additional phases (Cr/Ni two-phase shell, Cr silicide particles and Al-rich particles distributed in Ni_2Al_3) are found in the shells of pack-aluminized Ni–20 wt.% Cr wires with similar diameters. Fully homogenous Ni–Al and Ni–Cr–Al wires are achieved by interdiffusion at 1200 °C between the deposited Al-rich intermetallic shells and the Ni-rich core of both types of wires. Upon subsequent aging at 900 °C, wires with γ/γ′ structure and high hardness indicative of precipitation strengthening are obtained.

1. Introduction

Periodic cellular metals are of interest due to their low density, high specific mechanical properties, and high surface area [1–6]. These properties make them candidate materials for various structural and thermal applications. The most studied examples are honeycomb structures [2] and lattice-block structures [2–6], which are often used as the core of sandwich panels. Recent advances in weaving and braiding technologies make it possible to produce periodic cellular metals from metallic wires with various architectural features [6–8], with and without bonding at the wire contact points. These open-porosity wire structures could find applications in the aerospace industry due to their low density and high surface area, provided that they can be produced from high-temperature alloys resistant to oxidation, creep deformation and microstructure evolution (coarsening), in particular nickel-based superalloys. Since weaving and braiding require that the wires sustain high bending angles, it is very difficult to fabricate woven or braided structures from commercial nickel-based superalloy wires due to their limited ductility at room temperature. A solution to this problem is to fabricate woven or braided structures from ductile pure nickel wires and subsequently alloy these wires in the final structure to achieve nickel-based superalloy composition. Alloying can occur in the gas-phase, using pack cementation, which can deposit uniform metallic coatings up to several hundred micrometers in thickness on bulk Ni-based superalloys [9–13]. Many studies have been conducted on the formation mechanisms of nickel aluminide coatings by pack cementation of nickel with aluminum [11–14]. One of the earlier studies by Goward and Boone [11] reported inward and outward diffusion mechanisms involved in the formation of nickel aluminide phases by high-activity or low-activity cementation packs, and these observations have been supported by other researchers [12–14]. For coating formation in high-activity packs where Ni_2Al_3 is the main phase created, the inward Al diffusion dominated the process. Conversely, for low-activity packs where the main coating phase is NiAl (with a wide stoichiometric range of 21–38 wt.% or 37–57 at.% Al content at 1000 °C), outward Ni diffusion is the dominant mechanism, except for near-equiatomic NiAl, where Ni and Al diffuse at the same rates [15].

Pack-cementation alloying was recently demonstrated for open-cell Ni foams whose hollow struts, with near random spatial orientation and connectivity, were coated with Al- and/or Cr-rich phases [16–19]. Upon homogenization, these phases were dissolved into the nickel struts (~84 μm wall thickness) to create Ni–Cr [16] and Ni–Cr–Al foams [17], where the latter displayed the γ/γ′ structure typical of Ni-based superalloys after precipitation-aging or, for higher Al contents, the NiAl structure [18,19]. Pang et al. [20] used the pack cementation technique to synthesize open-

* Corresponding author. Tel.: +1 (847) 467 2595.
E-mail addresses: d-erdeniz@northwestern.edu (D. Erdeniz), dunand@northwestern.edu (D.C. Dunand).

http://dx.doi.org/10.1016/j.intermet.2014.02.009
0966-9795/

cell Ni–Fe–Cr foams. A similar approach was used by Johnson et al. [21], who added Al to various Ni-alloy sheets, with a thickness of 200 μm to 1 mm, by pack cementation and subsequently homogenized and aged to create γ′ precipitates. Burns et al. [22] followed a similar path to aluminize electrodeposited LIGA nickel specimens with a thickness of 100–200 μm. They also homogenized and aged these structures for γ′ strengthening.

In the present study, we investigate the kinetics of aluminization from various aluminum pack cementation sources, and subsequent homogenization, in ductile Ni and Ni–20 wt.% Cr wires which are suitable for woven or braided wire-based structures. The wires are subsequently aged to create strengthening by the precipitation of γ′ particles within a γ matrix. Micro-Vickers hardness tests are conducted to evaluate the change in mechanical properties after each processing step.

2. Experimental procedures

2.1. Alloying process

Wires used in this study were commercially pure nickel wires (99.95% pure Ni, procured from MWS Wire Industries) with a diameter of 127 μm and nichrome wires (Ni–20Cr–1Si–0.5Fe, wt.%, labeled here Ni–20Cr for the sake of brevity, procured from Alfa Aesar) with a diameter of 143 μm.

Four pack mixtures were employed with various Al activities, using the same filler (82 wt.% Al_2O_3 powder, 20–50 μm particle size, procured from Alfa Aesar) and activator (3 wt.% NH_4Cl powder, 100 μm particle size, procured from Alfa Aesar). The four Al sources were pure Al, Raney-Ni precursor (Ni–50 wt.% Al, 150 μm particle size, procured from Alfa Aesar), Ni_2Al_3 (Ni–40 wt.% Al, 150 μm particle size, procured from Goodfellow) and Ni–20 wt.% Al alloy powders (100–300 μm particle size, arc melted and crushed by ball milling), which are hereafter labeled as P100, P50, P40, and P20, respectively. The powder packs were mechanically mixed for ~30 min and 25 g of powder mixture was poured in an Al_2O_3 crucible. Five wire specimens, each with a length of 30–40 mm, were embedded within the center of the pack. To avoid contact with molten Al when P100 was used, the wires were covered with an additional thin layer of Al_2O_3 powders.

Aluminization experiments were carried out in a tube furnace under continuous Ar flow at 1000 °C. The filled crucible closed with a tight-fitting Al_2O_3 lid was pushed into the hot zone of the furnace preheated to 1000 °C and held there for 5–60 min. The time count was started as soon as the crucible reached the hot zone of the furnace, which caused a sudden drop of temperature at the thermocouple of ~45 °C. It took ~6 min for the crucible to reach 990 °C and an additional ~4 min to reach the set temperature of 1000 °C. At the end of the process, the crucible was pulled back to the water-cooled end of the tube furnace; cooling to 600 °C (a temperature where aluminization is negligible) took several minutes due to the thermal mass of the crucible. Specimens were retrieved from the pack and ultrasonically cleaned in acetone to remove pack material from their surface. Select wires were sealed in stainless steel tubes filled with Al_2O_3 powders, which were encapsulated under vacuum in quartz tubes. These encapsulated specimens were homogenized in a box furnace at 1200 °C for 48 h and aged at 900 °C for 8 h. Each heat treatment was terminated by water quenching.

2.2. Characterization

All wires were mounted in epoxy and prepared for microscopy by standard metallographic techniques. Polished cross-sections were chemically etched for 30 s with a mixture of 33 vol.% nitric acid, 33 vol.% acetic acid, 33 vol.% deionized water, and 1 vol.% hydrofluoric acid to reveal the γ/γ′ microstructure. A Hitachi S4800 scanning electron microscope equipped with an energy dispersive X-ray spectrometer (EDS) was used for imaging and chemical analysis. The EDS signal was calibrated by using standard samples of Ni_2Al_3 and Ni–20 wt.% Cr.

The compositions of the wires were calculated by measuring the average thicknesses of the nickel aluminide shells and the diameters of the wires. For each time step, micrographs of three different specimens were used and for each micrograph, ten shell thickness and ten diameter measurements were taken with the ImageJ digital image analysis software [23]. By utilizing the thickness and diameter values, area fractions of each phase were calculated and multiplied by the density and Al content of that phase (assuming an average Ni–41 wt.% Al or Ni–60 at.% Al composition for Ni_2Al_3, Ni–33 wt.% Al or Ni–52 at.% Al composition for NiAl, and Ni–13 wt.% Al or Ni–25 at.% Al composition for Ni_3Al),

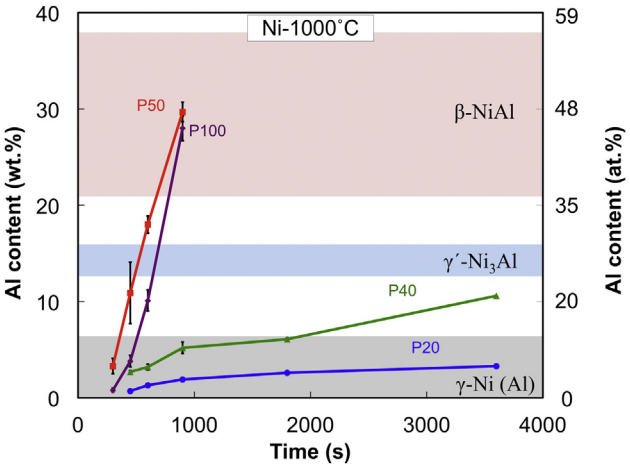

Fig. 1. Kinetics of aluminum mass gain (expressed as average wire aluminum content) for Ni wires aluminized at 1000 °C with P20, P40, P50, and P100 packs. The colored bands designate the phase boundaries at 1000 °C [24]. (For interpretation of the references to color in this figure legend, the reader is referred to the web version of this article.)

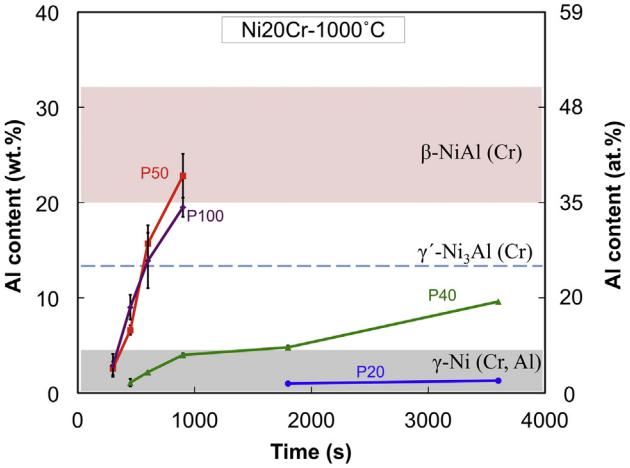

Fig. 2. Kinetics of aluminum mass gain for Ni–20Cr wires aluminized at 1000 °C with P20, P40, P50, and P100 packs. The colored bands designate the phase boundaries at 1000 °C [25]. The Ni–20Cr wires cannot fully transform into γ′-Ni_3Al due to the limited solubility of Cr in this phase, hence the phase is shown as a dashed line. (For interpretation of the references to color in this figure legend, the reader is referred to the web version of this article.)

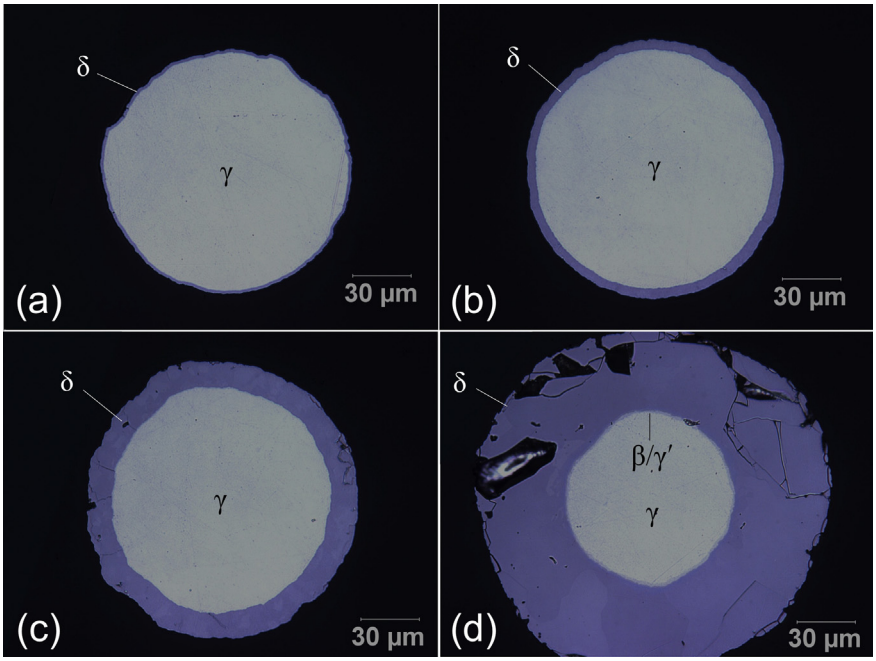

Fig. 3. Optical micrographs of cross-sections of Ni wires aluminized in P100 for (a) 300 s, (b) 450 s, (c) 600 s, (d) 900 s. The darker, outer shell is δ-Ni_2Al_3 and the lighter, inner core is γ-Ni. In (d), a thin β-NiAl/γ′-Ni_3Al shell is visible. The phases δ-Ni_2Al_3, β-NiAl, γ′-Ni_3Al and γ-Ni phases are marked with their Greek letters. Damage (cracks and voids) is due to metallographic preparation.

given in Refs. [24 and 25]. For the ternary system with complex coating microstructures, an overall composition of the coating was obtained by EDS for P100 and P50 packs and utilized in the calculations. EDS was also used to measure the compositions of homogenized and aged specimens. Micro-Vickers hardness tests were conducted on polished cross-sections with a Struers Duramin 5 hardness tester by applying a 136° pyramidal diamond indenter under a load of 100 g for 10 s.

3. Results and discussion

3.1. Processing

Figs. 1 and 2 show aluminum mass gain, expressed as average wire aluminum content, for Ni and Ni–20Cr wires as a function of aluminization time at 1000 °C in all four packs. For all packs, the Al mass gain rate is slower for Ni–20Cr wires than for Ni wires,

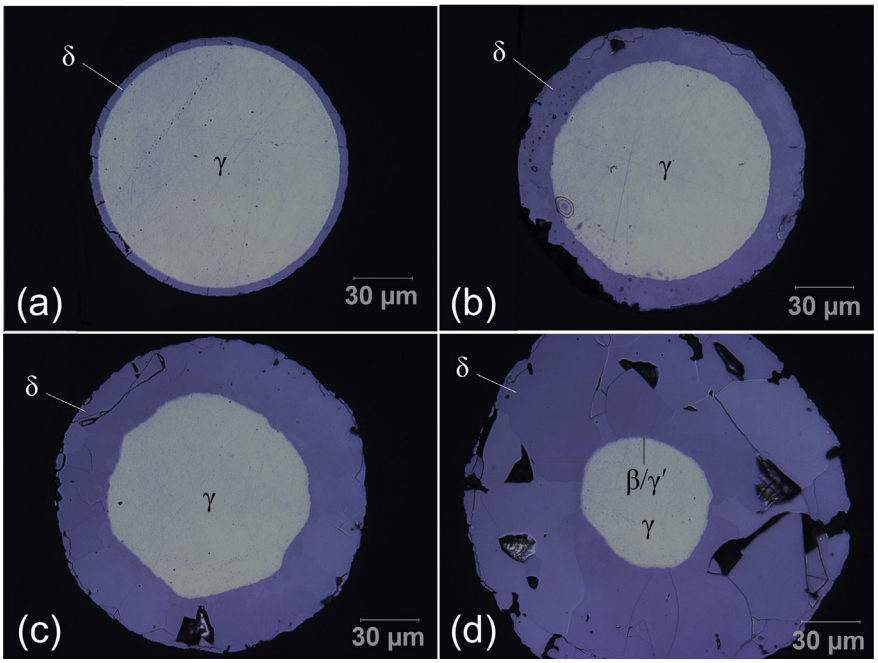

Fig. 4. Optical micrographs of cross-sections of Ni wires aluminized in P50 for (a) 300 s, (b) 450 s, (c) 600 s, (d) 900 s. In (d), a thin β-NiAl/γ′-Ni_3Al shell is visible. The phases are the same as in Fig. 3 and damage is due to metallographic preparation.

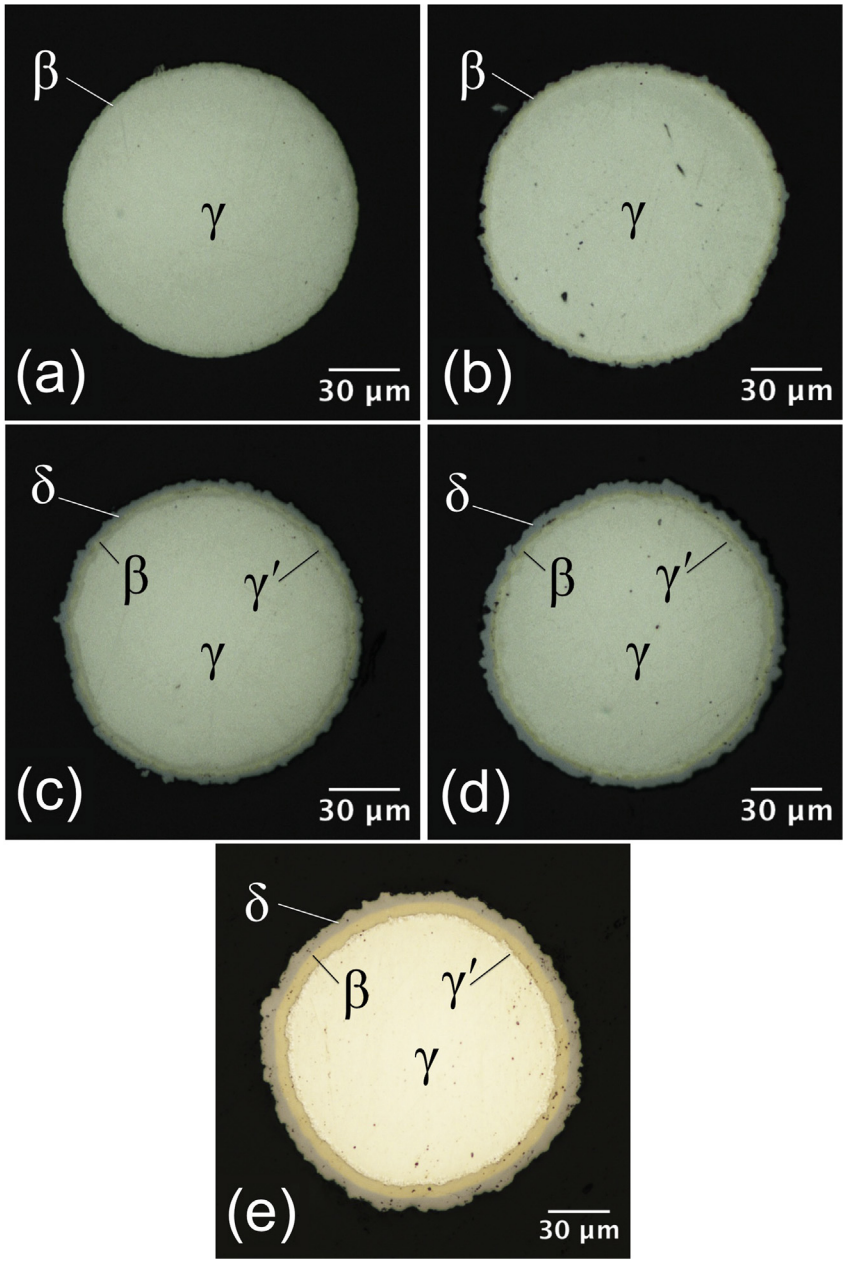

Fig. 5. Optical micrographs of cross-sections of Ni wires aluminized in P40 for (a) 450 s, (b) 600 s, (c) 900 s, (d) 1800 s, (e) 3600 s. The phases are the same as in Fig. 3.

e.g., there is a difference of 28% in P100 pack after 10 min. Jackson and Rairden [26] observed a similar effect in a study where Ni–Cr bulk alloys with 20–35 wt.% Cr were subjected to pack cementation at 1160 °C with an Al source similar to P100. The authors observed 11% lower diffusivity of Al atoms in Ni–35Cr as compared to Ni–20Cr [26]. Figs. 1 and 2 also show that the aluminization kinetics are almost the same for P100 and P50 packs, within error, for both Ni and Ni–20Cr wires, despite the lower Al activity in P50. The wires showed varying shell thicknesses over their lengths when imaging multiple cross-sections. These variations are expressed in the relatively large error bars in Figs. 1 and 2 for wires aluminized in P100 or P50. Variations in shell thicknesses will cause compositional differences along the wire upon homogenization, which may however be reduced by longitudinal diffusion. Figs. 1 and 2 further reveal that the Al mass gain is much slower for P20 and P40 than for P50 and P100, as expected from the lower Al activity. For both P20 and P40 packs, micrographs show that the shell thickness is nearly uniform among three cross-sections in a given wire and between three wires subjected to the same coating time. Thus, despite their slower deposition rates, P20 and P40 packs are probably preferable to the fast-depositing P100 and P50 packs since their uniform coatings avoid compositional (and thus microstructure and strength) fluctuations in the homogenized and aged wires.

As shown in Figs. 1 and 2, the wires treated for 450 s in P50 (similar to P100) had average Al contents of 11 wt.% for Ni wires and 7 wt.% for Ni–20Cr wires, which falls within the γ/γ' two-phase region at the aging temperature of 900 °C (7.5–11 wt.% Al for Ni and 3–6 wt.% Al for Ni–20Cr). Therefore, fine γ' precipitates, typical of superalloy microstructure, are expected upon homogenization and aging. Ni and Ni–20Cr wires treated in P40 would require ~30–60 min to reach that composition range. Neither of these wires

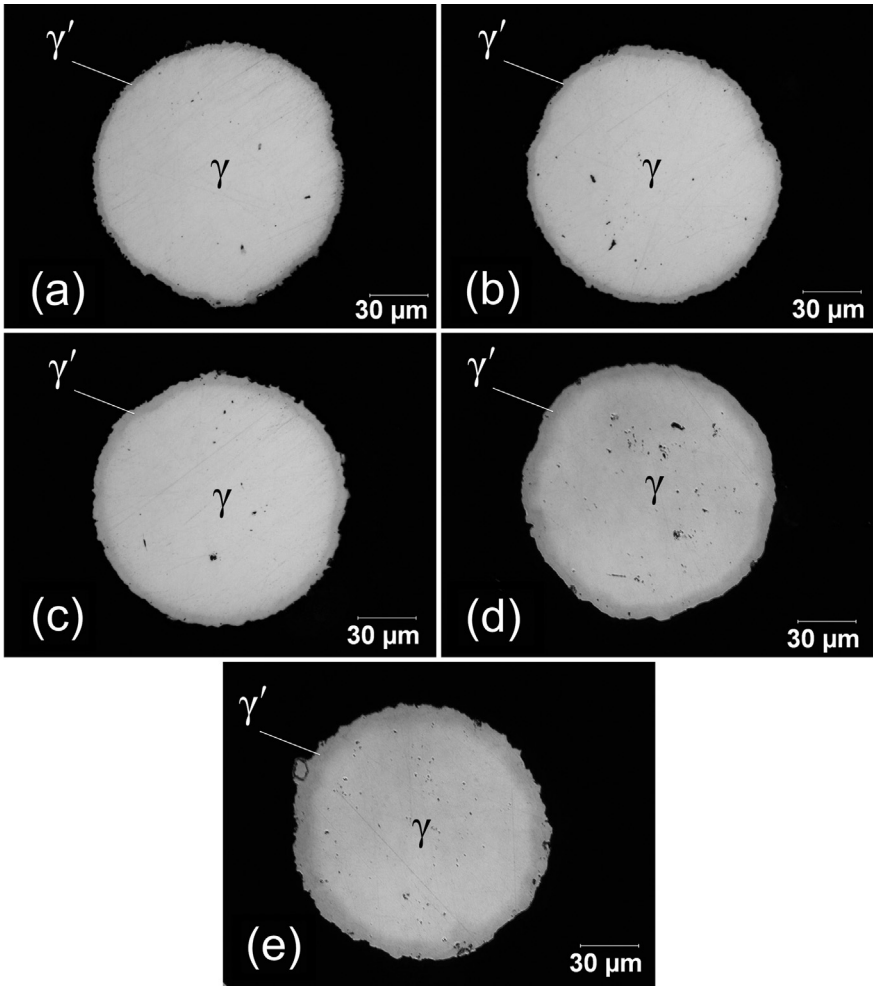

Fig. 6. Optical micrographs of cross-sections of Ni wires aluminized in P20 for (a) 450 s, (b) 600 s, (c) 900 s, (d) 1800 s, (e) 3600 s. The phases are the same as in Fig. 3.

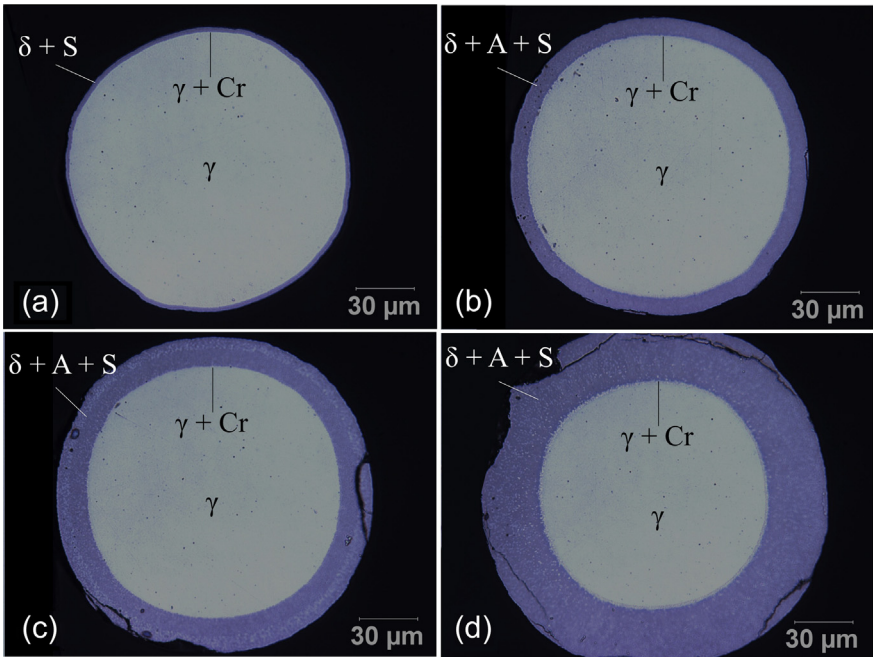

Fig. 7. Optical micrographs of cross-sections of Ni–20Cr wires aluminized in P100 for (a) 300 s, (b) 450 s, (c) 600 s, (d) 900 s. The phases are labeled as δ: Ni_2Al_3(Cr), β: NiAl(Cr), γ: Ni–20Cr, A: $Cr_{9.5}Al_{16}$, S: chromium silicide.

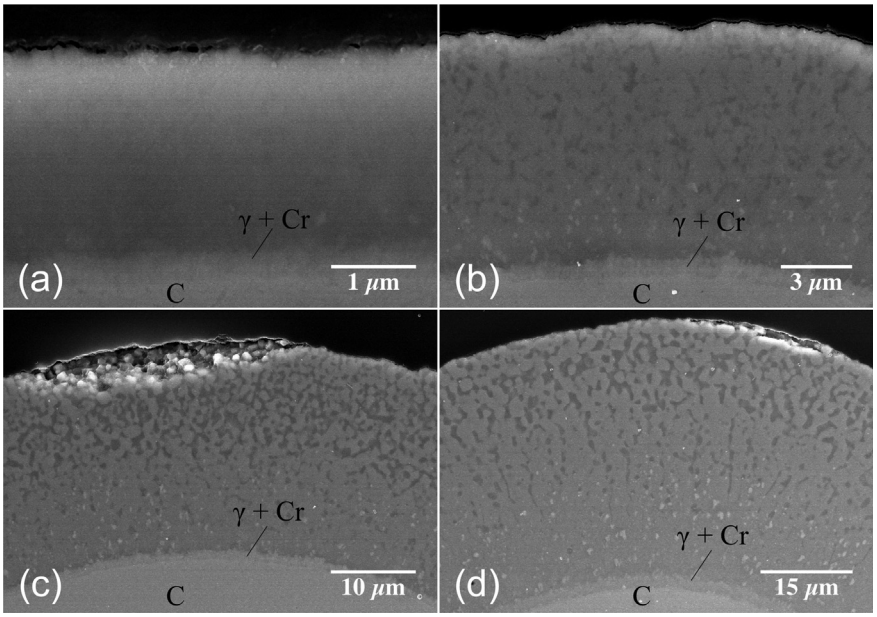

Fig. 8. Series of SEM images (with decreasing magnification) showing the shell on a cross-section of Ni–20Cr wires aluminized in P100 at 1000 °C for (a) 300 s, (b) 450 s, (c) 600 s, and (d) 900 s. The shell consists of a light gray matrix (δ-Ni_2Al_3); darker gray micron-size $Cr_{9.5}Al_{16}$ particles; and light-colored, submicron, chromium silicide particles. The interlayer between the shell and the core (C) is a mixture of fcc γ-Ni(Cr,Al) and bcc-Cr(Ni,Al).

achieved compositions close to the γ/γ′ range in the P20 pack after the longest time studied, 1 h.

Wire lengths were measured before and after the pack cementation. For all cases, no length changes or distortions were observed, which suggests that the formation of the Al-rich shells did not cause significant transient or residual stresses in the wires despite the large volume increases associated with the Al deposition and the creation of phases with densities lower than nickel. This is likely because of rapid creep relaxation of these phases, which are created at a temperature close to their melting points (1134 °C for Ni_2Al_3, 1134–1643 °C for NiAl, and 1370 °C for Ni_3Al.)

3.2. Microstructure

3.2.1. Aluminized Ni wires

Fig. 3(a)–(d) shows Ni wires aluminized in P100 at 1000 °C for 300, 450, 600, and 900 s, respectively. All wires exhibited a Ni_2Al_3 shell with a thickness between 2 and 51 μm depending on the processing time, which showed cracks, most likely due to metallographic preparation of the very brittle Ni_2Al_3 intermetallic phase. The wire core is nickel and contains some Al, which was detected by EDS to a depth of 4 μm from the Ni_2Al_3 interface for the sample aluminized for 450 s. The maximum solubility of Al in Ni at the

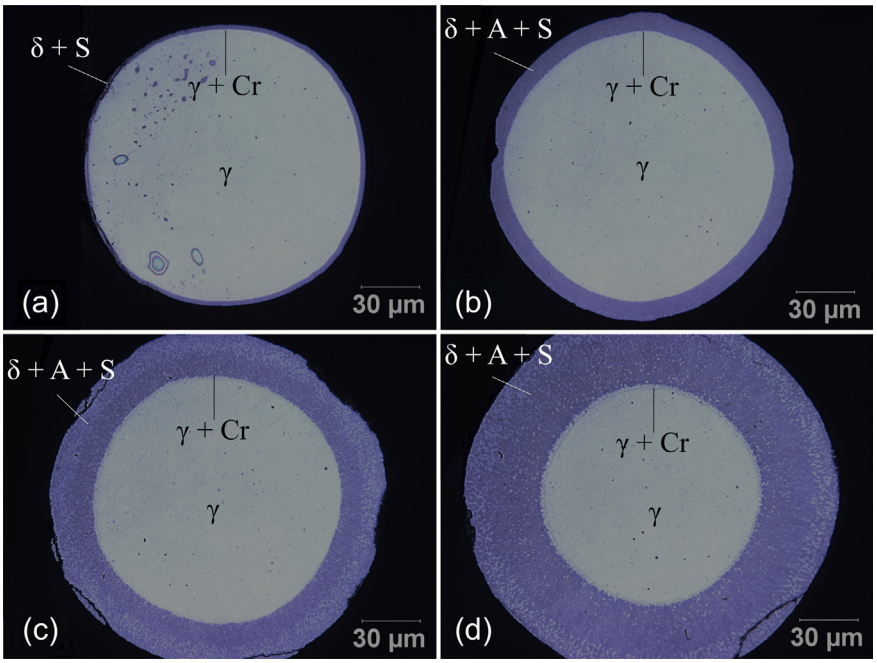

Fig. 9. Optical micrographs of cross-sections of Ni–20Cr wires aluminized in P50 for (a) 300 s, (b) 450 s, (c) 600 s, (d) 900 s. The phases are labeled as in Fig. 7.

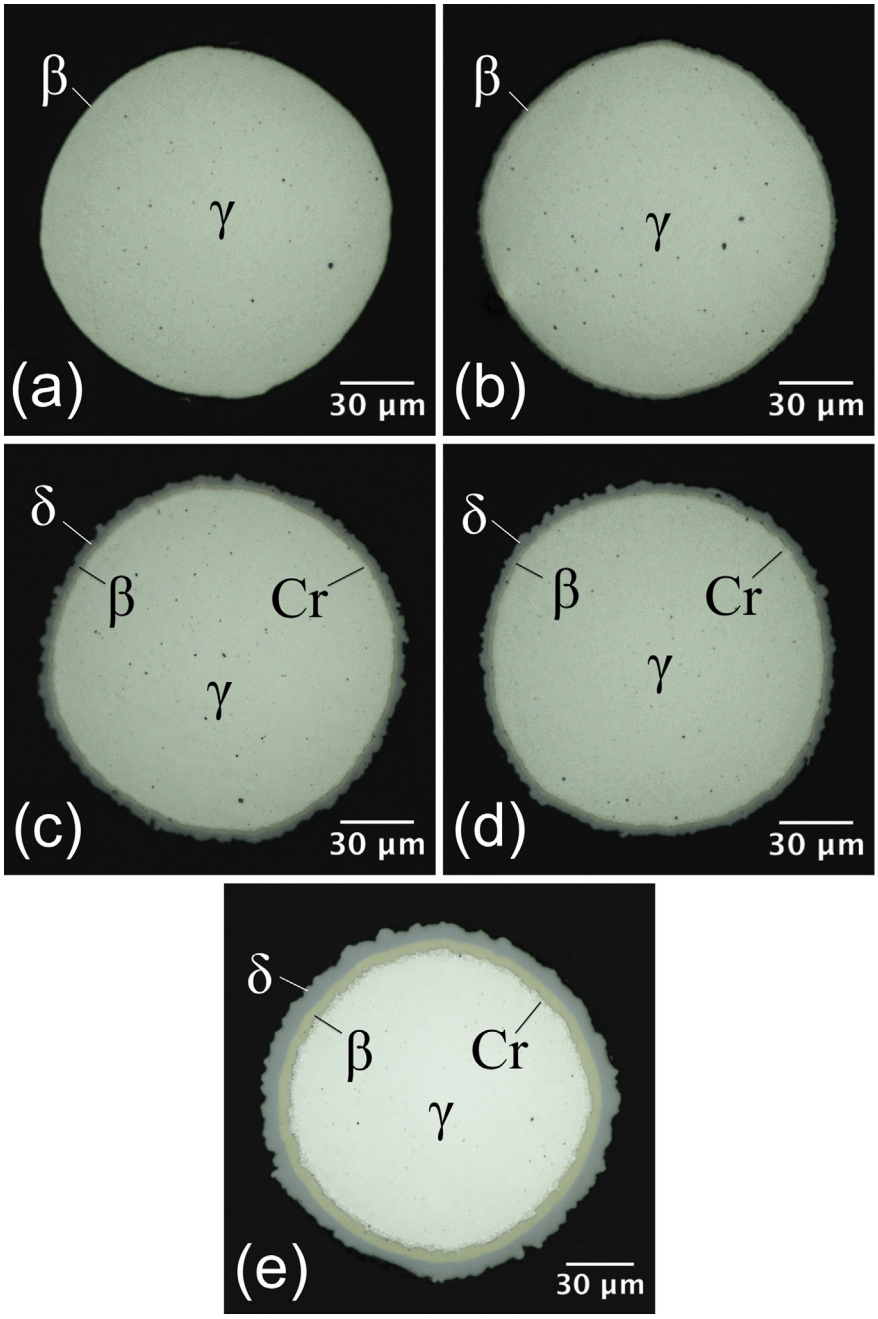

Fig. 10. Optical micrographs of cross-sections of Ni–20Cr wires aluminized in P40 for (a) 450 s, (b) 600 s, (c) 900 s, (d) 1800 s, (e) 3600 s. The phases are labeled as in Fig. 7. A Cr rejection layer is also marked at the β/γ interface.

processing temperature is 7.5 wt.% [24]. Two thin shells of NiAl and Ni_3Al (<1 μm wide) located between the Ni core and the outer Ni_2Al_3 shell are visible in Fig. 3(d) for the longest aluminization time, but not on the other optical micrographs (however, these shells are visible on SEM micrographs). The formation of thin layers of NiAl and Ni_3Al was expected from various studies, which report that high-activity Al packs create thick Ni_2Al_3 shells with thin (~1 μm) NiAl/Ni_3Al intermediate shells [11–14,17–19].

Fig. 4(a)–(d) depicts Ni wires aluminized in P50 at 1000 °C for 300, 450, 600, and 900 s, respectively. All wires have a microstructure very similar to that of the wires aluminized in P100 (Fig. 3(a)–(d)). The Ni_2Al_3 shell grows from 4 to 56 μm as the processing time increases. This was unexpected, since previous studies [13,17] showed that the use of P50 as the Al source creates NiAl coatings only. However, those studies were conducted with bulk Ni-based superalloy specimens [13] or with Ni foams [17], where the specimen surface area per unit volume was significantly lower than the wire specimens. Therefore, for the present wires, it is possible that the relatively high specific surface area favored the formation of the Al-richer phase Ni_2Al_3 phase. Furthermore, as in Fig. 3(d), the wire aluminized for the longest time also shows thin (<1 μm) NiAl and Ni_3Al intermediate shells (Fig. 4(d)). Formation of the same nickel aluminide phase, Ni_2Al_3, with both P100 and P50 supports the very similar mass gain rates found in Figs. 1 and 2 and discussed in the previous section. Since the surface composition determines the diffusion driving force and thus the diffusion

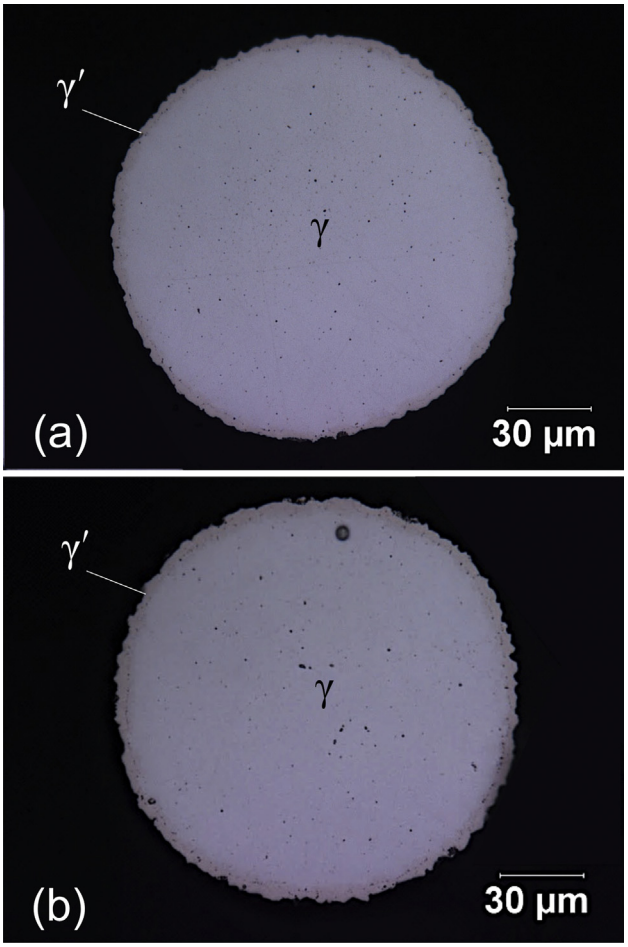

Fig. 11. Optical micrographs of cross-sections of Ni–20Cr wires aluminized in P20 for (a) 1800 s, (b) 3600 s, showing the γ′-Ni_3Al and fcc γ-Ni–20Cr phases.

kinetics, and since the Ni_2Al_3 phase has a narrow composition range, it is expected that the aluminization rates are the same for both packs [19]. Therefore, the much lower aluminization rates for P40 and P20 indicate that an aluminide phase with lower Al content than Ni_2Al_3 is expected. This prediction is indeed fulfilled, as described below.

Fig. 5(a)–(e) shows Ni wires aluminized in P40 at 1000 °C for 450, 600, 900, 1800, and 3600 s. At the early stages (450–600 s), the wires displayed a thin (~3–4 μm) NiAl shell. After 900 s, a thin (~3.5 μm) outer shell of Ni_2Al_3 becomes visible along with a 2 μm shell of NiAl and a 2 μm inner shell of Ni_3Al. For 1800 and 3600 s, all three shells grow larger. Overall Al gain in P40 was significantly lower than in P100 and P50 packs due to the lower activity of Al, as evidenced by the smaller shell thicknesses and the lower Al content of the main phase (NiAl).

Fig. 6(a)–(d) shows Ni wires aluminized in P20 at 1000 °C for 450, 600, 900, 1800, and 3600 s. The wires show an outer shell of Ni_3Al growing with aluminization time, in contrast to the previous packs, where Al-richer phases were created (Ni_2Al_3 for P50 and P100 or NiAl for P40). To the best of our knowledge, this is the first report of the formation of a Ni_3Al coating via pack cementation. The shell maintained its integrity during sample preparation since Ni_3Al is more ductile than Ni_2Al_3 at room temperature. Such a Ni_3Al shell, which is at equilibrium with the Ni core (i.e. no intermediate phase exists between Ni and Ni_3Al), might be useful for other Ni-based objects, both micro and macroscopic, as the Ni_3Al phase is quite ductile at moderate and elevated temperature and provides enhanced oxidation resistance.

3.2.2. *Aluminized Ni–20Cr wires*

In Fig. 7a–d, Ni–20Cr wires are shown after aluminization in P100 at 1000 °C for 300, 450, 600, and 900 s, respectively. The shell consists of a Ni_2Al_3 matrix (growing from 1 to 32 μm in thickness as time increases) containing micron-size Al-rich particles, possibly the $Cr_{9.5}Al_{16}$ phase, which is in equilibrium with Ni_2Al_3 and an Al-rich liquid according to the ternary phase diagram [25]. As illustrated in Fig. 8a–d, these darker-gray particles become visible after 450 s and grow with aluminization time; at any given time, they are larger closer to the wire surface, where they formed first and were thus able to coarsen longer. Closer to the Ni–20Cr core, lighter-colored submicron particles are visible, which are probably one of

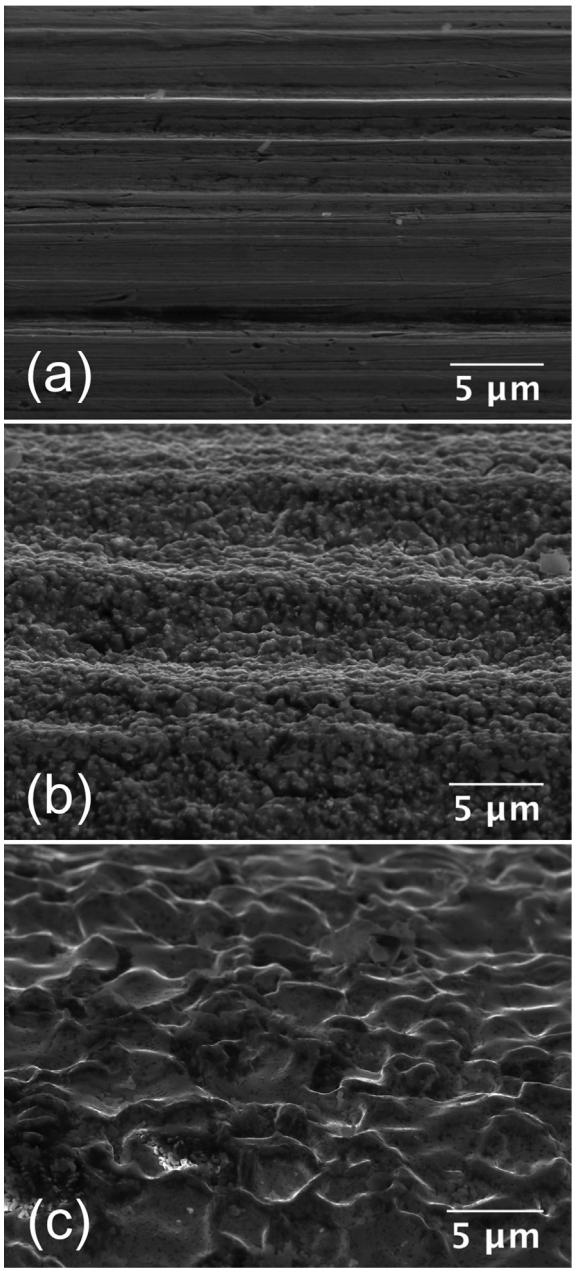

Fig. 12. SEM micrographs showing surface features of (a) as-received Ni wire, and Ni wires aluminized for 600 s in (b) P100, (c) P40.

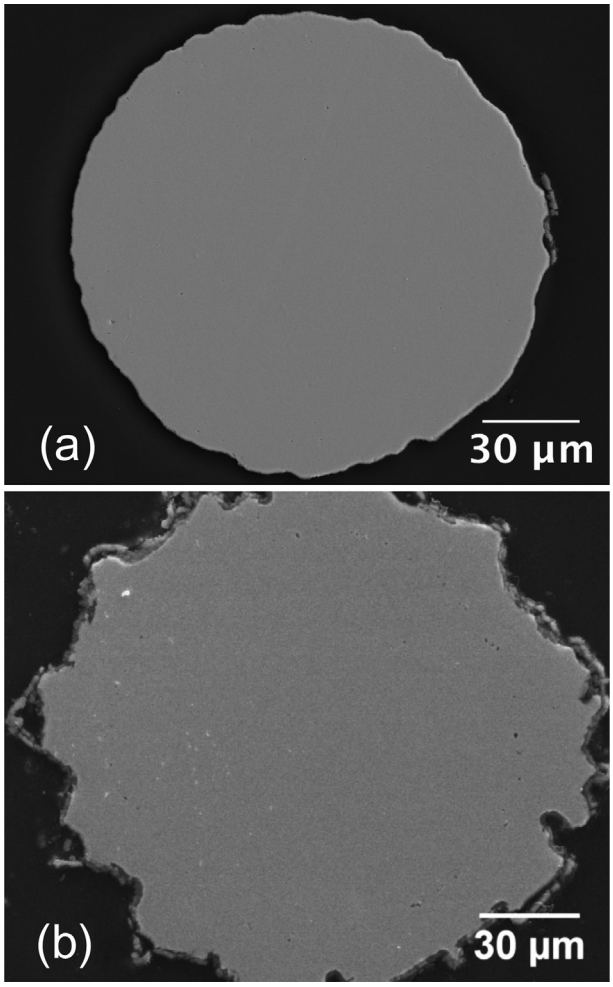

Fig. 13. Optical micrographs of cross-sections of homogenized wires (a) Ni–9Al (wt.%, P50 – 450 s), (b) Ni–19Cr–6Al (wt.%, P50 – 450 s).

the chromium silicide phases. Due to their small size, the exact composition of both types of particles could not be ascertained by EDS, however increased peak intensity for Cr and Si elements were observed. There is also a thin Ni–49Cr–11.5Al (wt.%) layer between the Ni_2Al_3 shell and the Ni–20Cr core. This thin layer composition falls in the fcc-Ni(Cr,Al) and bcc-Cr(Ni,Al) two-phase field of the Ni–Al–Cr phase diagram [25], but the expected Cr(Ni,Al) particles (bcc-Cr with Ni and Al in solid solution) are not resolved in Fig. 8(a)–(d).

Fig. 9(a)–(d) shows Ni–20Cr wires aluminized in P50 at 1000 °C for 300, 450, 600, and 900 s, respectively. No microstructural differences are observed between the Ni–20Cr wires treated in P100 and P50, as is also the case for Ni wires. Similar to the Ni wires aluminized in P100 and P50, the Ni_2Al_3(Cr) shell in Fig. 9(a)–(d) was cracked and pulled out during metallographic preparation due to the very brittle nature of that phase at room temperature.

Ni–20Cr wires aluminized in P40 at 1000 °C for 450, 600, 900, 1800, and 3600 s, respectively are shown in Fig. 10(a)–(e). At the early stages, a thin NiAl(Cr) shell is observed. After 900 s, a Ni_2Al_3(Cr) shell becomes visible at the outer surface. Finally, after 3600 s, the specimen exhibits a 8 μm thick Ni_2Al_3(Cr) shell, a 5 μm shell of NiAl(Cr), and a 2 μm layer of rejected bcc-Cr(Ni,Al). Unlike the P100 and P50 packs, the aluminide coating had less than 5 wt.% Cr and the rejection layer was rich (>90 wt.%) in Cr.

Fig. 11(a) and (b) shows Ni–20Cr wires aluminized in P20 at 1000 °C for 1800 s and 3600 s, respectively. No shells were visible for the 300–900 s treatments, indicating that the shell, if it exists, is below the 1 μm resolution of the optical microscope. After longer aluminization times (1800 and 3600 s), a Cr-free γ′-Ni_3Al shell, similar to the Ni-P20 specimens, was observed with a maximum thickness of 4 μm.

Fig. 12(a)–(c) shows the surface of the as-received Ni wire and Ni wires aluminized in P100 and P40 packs for 600 s. The surface structure of the wires aluminized in P50 and P20 are not shown, as they are nearly identical to those aluminized in P100 and P40, respectively. The wires aluminized in P100 and P50 (Fig. 12(b)) show long troughs that may be the troughs present in the drawn structure (Fig. 12(a)); these troughs are absent in the wires aluminized in P40 and P20 (Fig. 12(c)), possibly because surface diffusion was faster and filled the troughs. The surface structures of the aluminized Ni–20Cr wires in all packs were nearly identical with those of the aluminized Ni wires and are thus not shown here.

3.2.3. Homogenization and aging of aluminized wires

Fig. 13(a) shows a fully homogenized Ni–9Al (wt.%) wire, which was aluminized in P50 pack for 450 s. Fig. 13(b) shows a fully homogenized Ni–19Cr–6Al (wt.%) wire, which was aluminized in P50 pack for 450 s. The Ni–Cr–Al wires exhibited rough surfaces, probably due to the formation of Kirkendall pores and their migration to the surface. No Kirkendall pores within the Ni–Cr–Al wires were observed below 6 wt.% Al, which is the maximum target composition for the γ/γ′ structure [25]. If a smooth surface was necessary in the Ni–19Cr–6Al (wt.%) wire shown in Fig. 13(b), it could be obtained by etching.

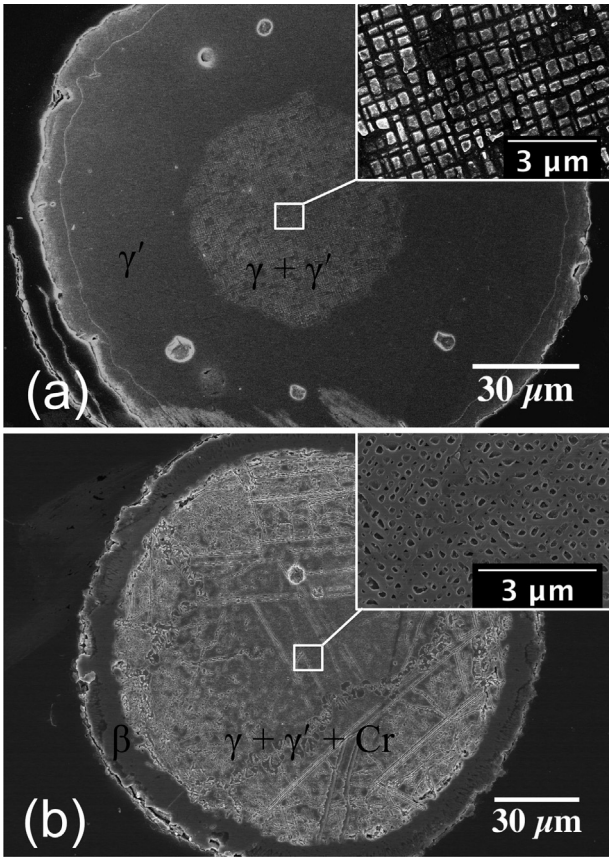

Fig. 14. SEM micrographs of etched cross-sections of homogenized and aged wires showing a γ-γ′ microstructure in inset for (a) Ni–12Al (wt.%, P50 – 450 s) (b) Ni–19Cr–8Al (wt.%, P50 – 480 s).

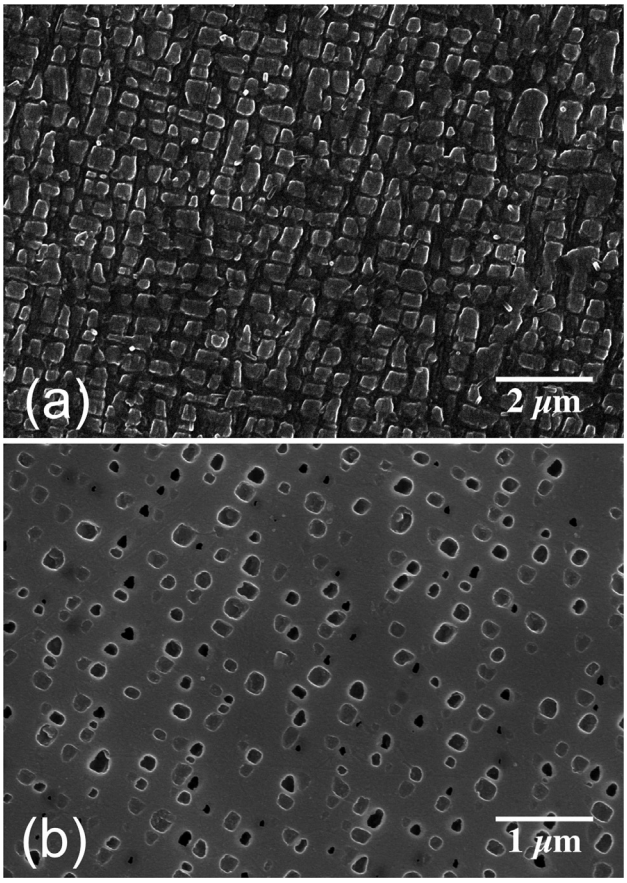

Fig. 15. SEM micrographs of etched γ-γ′ microstructure found throughout the cross-sections of (a) Ni wire aluminized (P50 – 360 s), homogenized and aged, with a final composition of Ni–10Al (wt.%) and (b) Ni–20Cr wire aluminized (P50 – 420 s), homogenized and aged, with a final composition of Ni–19Cr–4.5Al (wt.%). Cuboidal γ′ precipitates are distributed in a γ matrix phase.

Fig. 14(a) and (b) shows γ′ precipitates in wires with higher Al contents than those in Fig. 13(a) and (b): Ni–12Al (wt.%) in Fig. 14(a) and Ni–19Cr–8Al (wt.%) in Fig. 14(b), both aged at 900 °C for 8 h after homogenization. The compositional difference between the samples shown in Figs. 13(a) and 14(a), despite being treated under the same conditions, is due to the varying shell thicknesses of the as-coated wires. The precipitates in the Ni–Al wire are concentrated at the core of the wire, where the overall composition is Ni–10 wt.% Al, while the outer shell is single-phase γ′-Ni_3Al (Ni–13 wt.% Al). The existence of this mixed microstructure is due to the high Al content. According to the phase diagram [24], to obtain a γ/γ′ microstructure at 900 °C, the overall Al content cannot exceed 11 wt.%. The precipitates in the Ni–Al wire core (Fig. 14(a)) had a cuboidal morphology and a volume fraction of ~55%, as determined by image analysis. The Ni–Cr–Al wire had a more complex microstructure (Fig. 14(b)). Its shell consists of NiAl(Cr) while its core is γ/γ′ with precipitated Cr(Ni,Al). The main second phase present in the wire core is also in the form of γ′ precipitates that had a cuboidal morphology with a volume fraction of ~22%.

Fig. 15(a) and (b) shows wires with γ/γ′ microstructure extending over their whole cross-sections. The Ni–10Al (wt.%) wire shown in Fig. 15(a) was obtained by aluminizing in P50 pack for 360 s. Upon homogenization and aging, the wire displayed cuboidal γ′ precipitates with an average size of 400 nm and a volume fraction of ~55%. The Ni–19Cr–4.5Al (wt.%) wire shown in Fig. 15(b) was obtained by aluminizing in P50 pack for 420 s. The cuboidal γ′ precipitates had an average size of 220 nm and a volume fraction of ~15%.

3.3. Hardness evolution

Hardness values of the wires were measured at various stages within the process; an estimate (in MPa) of the ultimate tensile strength (UTS) is given by tripling the Vickers hardness value, as widely used for a variety of metals including pure nickel [27,28].

As-received Ni and Ni–20Cr wires, which were annealed at 1200 C for 1 h, had hardness values of 117 ± 5 HV and 200 ± 11 HV, respectively. The 1.7 fold difference corresponds to the solid solution strengthening of Cr, and to a lesser extend Si and Fe. Reported hardness values are 90 HV for pure Ni and 160 HV for Ni–16wt.% Cr, both in bulk form and annealed condition [29].

The hardness of a homogenized Ni–7Al (wt.%) wire, with a composition within γ/γ′ phase field, was 171 ± 12 HV. This ~50% increase is due to the solid solution strengthening of Al in the homogenized state, as SEM observations showed no γ′ precipitation in this sample upon water quenching. The hardness of a Ni–10Al (wt.%) wire after subsequent aging at 900 °C for 8 h was 265 ± 5 HV. This more than doubling in hardness illustrates the effectiveness of precipitation strengthening.

Ni–19Cr–3Al alloy wires, with a composition within the γ/γ′ phase field, showed a hardness value of 206 ± 17 HV after homogenization. This value is similar to the 200 ± 11 HV of the annealed Ni–20Cr, as expected given the small amount of additional Al in solid solution. Another wire with a composition of Ni–19Cr–5Al, after the aging treatment, reached a hardness of 320 ± 12 HV (corresponding to a UTS of ~960 ± 36 MPa), illustrating the strong effect of precipitation strengthening.

All the aged wires exhibited uni-modal cuboidal microstructures. For optimum mechanical properties, duplex-size microstructures are preferred [30]. However, the aim of this study was to demonstrate the feasibility of creating γ′ strengthened Ni-based wires by pack cementation, and further microstructure development studies will be reported elsewhere.

4. Conclusions

Ni and Ni–20Cr wires with 127–143 μm diameter were pack-aluminized at 1000 °C for up to 1 h, resulting in Al addition of up to 30 wt.%.

For Ni wires, four different packs were employed with varying Al activities: (a) two packs with higher Al activities (P100 and P50) resulted in the formation of a main Ni_2Al_3 shell and very thin interlayers of NiAl and Ni_3Al; (b) a less active pack P40 formed all three phases with significant thicknesses; (c) the lower activity pack P20 formed a single Ni_3Al shell.

For Ni–20Cr wires, the same pack compositions were used for the same durations: (a) two higher Al activity packs (P100 and P50) resulted in the formation of a main Ni_2Al_3(Cr) outer shell that contained a mixture of other phases including chromium aluminide and silicide (from minor Si content in the original wires) precipitates. There was also an interlayer of Ni–49Cr–11.5Al (wt.%, expected to consist of fcc-Ni(Cr,Al) and bcc-Cr(Ni,Al)) between the outer shell and the Ni–20Cr core; (b) the less active P40 pack formed both Ni_2Al_3(Cr) and NiAl(Cr) phases with significant thicknesses after 450 s; (c) the low-activity P20 pack created a thin Ni_3Al layer after 0.5 and 1 h treatments. Wire surface images showed that with a decrease in pack Al activity, the surface quality increased.

Wires aluminized to 5–10 wt.% Al were fully homogenized at 1200 °C for 48 h and aged at 900 °C for 8 h. The aging treatment

formed γ′ precipitates distributed in the γ matrix phase. The aged Ni–10Al and Ni–19Cr–5Al wires had hardness values of 265 ± 5 HV (UTS ~ 795 ± 15 MPa) and 320 ± 12 HV (UTS ~ 960 ± 36 MPa), respectively, indicative of effective precipitation strengthening.

Acknowledgments

The authors acknowledge the financial support from the Defense Advanced Research Projects Agency under award number W91CRB1010004 (Dr. Judah Goldwasser, program manager). They also thank Prof. Peter Voorhees and Dr. Thomas Philippe (both Northwestern University), as well as Prof. Kevin Hemker (Johns Hopkins University) for useful discussions, Mr. Edward Lee Pang for his help with metallographic sample preparation, and Ms. Ashley Paz y Puente for proof reading.

References

[1] Evans AG, Hutchinson JW, Fleck NA, Ashby MF, Wadley HNG. The topological design of multifunctional cellular materials. Prog Mater Sci 2001;46:309–27.
[2] Wadley HNG. Multifunctional periodic cellular materials. Phil Trans R Soc A 2006;364:31–68.
[3] Nathal MV, Whittenberger JD, Hebsur MG, Kantzos PT, Krause DL. Superalloy lattice block structures. In: Green KA, Pollock TM, Harada H, Howson TE, Reed RC, Schirra JJ, et al., editors. Proceedings of the 10th International Symposium on Superalloys. PA: Champion; 2004. pp. 431–9.
[4] Fleck NA, Deshpande VS, Ashby MF. Micro-architected materials: past, present, and future. Phil Trans R Soc A 2010;466:2495–516.
[5] Schaedler TA, Jacobsen AJ, Torrents A, Sorensen AE, Lian J, Greer JR, et al. Ultralight metallic microlattices. Science 2011;334:962–5.
[6] Wadley HNG, Fleck NA, Evans AG. Fabrication and structural performance of periodic cellular metal sandwich structures. Compos Sci Technol 2003;63:2331–43.
[7] Lee Y-H, Lee B-K, Jeon I, Kang K-J. Wire woven bulk Kagome truss cores. Acta Mater 2007;55:6084–94.
[8] Mohamed MH, Bogdanovich AE, Dickinson LC, Singletary JN, Lienhart RB. A new generation of 3D woven fabric preforms and composites. SAMPE J 2001;37:8–17.
[9] Van Aller T, Treatment of metals, US 1,155,974, U.S. Patent Office, 1911.
[10] Gilson EG, Process of treating metals, US 1,091,057, U.S. Patent Office, 1913.
[11] Goward GW, Boone DH. Mechanisms of formation of diffusion aluminide coatings on nickel-base superalloys. Oxid Met 1971;3:475–95.
[12] Hickl AJ, Heckel RW. Kinetics of phase layer growth during aluminide coating of nickel. Met Trans A 1975;6:431–40.
[13] Das DK, Singh V, Joshi SV. Evolution of aluminide coating microstructure on nickel-base cast superalloy CM-247 in a single-step high-activity aluminizing process. Met Trans A 1998;29:2173–88.
[14] Goward GW, Cannon LW. Pack cementation coating for superalloys: a review of history, theory, and practice. J Eng Gas Turb Power 1988;110:150–4.
[15] Shankar S, Seigle LL. Interdiffusion and intrinsic diffusion NiAl (delta) phase of Al–Ni system. Met Trans A 1978;9:1467–76.
[16] Choe H, Dunand DC. Mechanical properties of oxidation resistant Ni–Cr foams. Mat Sci Eng A 2004;384:184–93.
[17] Choe H, Dunand DC. Synthesis, structure, and mechanical properties of Ni–Al and Ni–Cr–Al– foams. Acta Mater 2004;52:1283–95.
[18] Hodge AM, Dunand DC. Synthesis of nickel–aluminide foams by pack-aluminization of nickel foams. Intermetallics 2001;9:581–9.
[19] Dunand DC, Hodge AM, Schuh CA. Pack aluminization kinetics of nickel rods and foams. Mater Sci Tech 2002;18:326–32.
[20] Pang Q, Wu GH, Xiu ZY, Chen GQ, Sun DL. Synthesis and mechanical properties of open-cell Ni–Fe–Cr foams. Mat Sci Eng A 2012;534:699–706.
[21] Johnson SJ, Tryon B, Pollock TM. Post-fabrication vapor phase strengthening of nickel-based sheet alloys for thermostructural panels. Acta Mater 2008;56:4577–84.
[22] Burns DE, Zhang Y, Teutsch M, Bade K, Aktaa J, Hemker KJ. Development of Ni-based superalloys for microelectromechanical systems. Scr Mater 2012;67:459–62.
[23] Schneider CA, Rasband WS, Eliceiri KW. NIH image to ImageJ: 25 years of image analysis. Nat Methods 2012;9:671–5.
[24] Okamoto H. Phase diagrams for binary alloysIn Desk handbook, vol. 1; 2000.
[25] Chart T, Dinsdale A, Putland F. The NPL alloy databank: its use in the calculation of phase diagrams for superalloy development. Spec Publ – Chem Soc; 1980:235–45.
[26] Jackson MR, Rairden JR. Microstructure and chemistry of aluminide coating of Ni–Cr and Ni–Co–Cr alloys. J Vac Sci Technol 1980;17:81–4.
[27] Tabor D. A simple theory of static and dynamic hardness. P Roy Soc Lond A Mat 1948;192:247–74.
[28] Tabor D. The hardness and strength of metals. J Inst Met 1951;79:1–18.
[29] Louis FT. Mechanical properties of nickel and nickel alloys. In: Brandes EA, editor. Smithells metals reference book. England: Butterworth & Co Ltd.; 1983. pp. 22–69.
[30] Balikci E, Mirshams RA, Raman A. Tensile strengthening in the nickel-base superalloy IN738LC. J Mater Eng Perform 2000;9:324–9.